Journal of
Materials Chemistry C

Accepted Manuscript

This article can be cited before page numbers have been issued, to do this please use: Z. Peng, Z. Wang, Z. Huang, S. Liu, P. Lu and Y. Wang, *J. Mater. Chem. C*, 2018, DOI: 10.1039/C8TC02416B.

ROYAL SOCIETY OF CHEMISTRY

rsc.li/materials-c

View Article Online
DOI: 10.1039/C8TC02416B

Journal Name

ARTICLE

Expression of Anti-Kasha's emission from amino benzothiadiazole and its utilizations for fluorescent chemosensors and organic light emitting materials

Received 00th January 20xx,
Accepted 00th January 20xx

DOI: 10.1039/x0xx00000x

www.rsc.org/

Zhixing Peng, Zaibin Wang, Zongwei Huang, Shaojie Liu, Ping Lu*, Yanguang Wang*

Various amino benzothiadiazoles (**Am-BTDs**) are synthesized and their photophysical properties in different states (solution, film, crystal, and powder) are investigated. The unusual anti-Kasha's emission is observed for those compounds with strong electronic coupling effect between donor and acceptor which directly results in the white emission of those compounds in dilute solutions. Among these **Am-BTDs**, some of them can be utilized as fluorescent chemosensors in sensing gaseous ammonia, and some of them can be developed for detecting fluoride anion with high selectivity and high sensitivity. Moreover, aggregation causing quenching is not observed for these compounds in solids. They are emissive in films, crystals and powders with high color purity and moderate efficiencies. The emission color could be tuned from yellow to red according to the varied amino groups. Furthermore, they can be used as emissive layer in organic light emitting diodes.

Introduction

2,1,3-Benzothiadiazole (**BTD**) is a unique electron deficient heterocycle which has been widely applied as a building block in the synthesis of optoelectronic compounds for organic light emitting diodes (OLEDs),[1] organic field effect transistors (OFETs),[2] solution-processable bulk-heterojunction organic solar cells (BHJ-OSCs),[3] organic flow battery,[4] solar-hydrogen conversion,[5] bioprobes,[6] and fluoride anion chemsensors.[7] Connection of **BTD** with AIE-fluogen (aggregation induced emission active fluogen) induces these **BTD**-based compounds emitting light in aggregates for long-term two-photon cell imaging.[8] General speaking, the π-extended **BTD** derivatives facilitate planarization and polarization which enhance the electronic communication between electron donor and electron acceptor and simultaneously increase intermolecular interactions and afford well-ordered crystal structures for better device performance.[2a, 9] Meanwhile, most of **BTD**-based compounds are stable in both ground state and excited state even after long period of irradiation.[6a] Therefore, discovery the new **BTD**-based compounds in order to fit the requirement of the steady development of the material science and life science has always been the focus of research. By surfing the literature, the conjugation normally extends from 4,7-positions of **BTD** by covalently bonding alkenyl,[10] alkynyl,[11] and aryl.[1, 12] For example, insertion of **BTD** into polyfluorene backbone, a pure green emitter was approached.[12c] On the other hand, modification on the **BTD** core by installing electron-withdrawing fluoro or cyano on 5, or 6-position of **BTD** could further lower its lowest unoccupied molecular orbital level (LUMO) and thereafter increase the electron affinity for red-shifted absorption.[13-14] Instead of fluorination and cyanation, borylation could also lower the LUMO level and enhance the electron affinity.[15] On the other hand, substitution on 5, or 6-position of **BTD** with electron-donating alkoxy group changes them into transmitters by improving the electron mobility.[16] However, direct substitution on 4,7-positions with amino group is seldom reported although this kind of modification would dramatically change the energy level to a great extent and have been demonstrated for some particular purposes (Scheme 1). For instance, by covalently bonding 2-aminopyridine to 4-position of BTD, **BTD-AP** possesses dual functions of excited state intramolecular proton transfer (ESIPT) and intramolecular charge transfer (ICT) and has been applied as a mitochondria fluorescent marker with high selectivity and stability.[6b, 17] By attaching *p*-nitrophenylamino group on the 4-postion of BTD, **CBT-NH** shows selectivity and sensitivity to fluoride anion and works as a fluoride fluorescent chemosensor.[7] By incorporating with diarylamino, **MR-3** was designed for dye-sensitized solar cells with an apparently increment of the power conversion efficiency.[12c] Recently, **BTZ-DMAC** as well as others, with two diarylamino groups on 4,7-positions of BTD, have been designed for red TADF-emitters (thermally activated delay fluorescence emitters) with electroluminescence at 636 nm and a maximum external quantum efficiency of 8.8%.[18] Here, we would like to report the synthesis of a series of amino benzothiadiazole (**Am-BTDs**,

Department of Chemistry, Zhejiang University, Hangzhou 310027, P. R. China.
**E-mail: pinglu@zju.edu.cn, orgwyg@zju.edu.cn.*
Electronic Supplementary Information (ESI) available: structural characterization data, TGA, crystallographic data, photophysical spectra, DFT, CV. See DOI: 10.1039/x0xx00000x

1-7), the investigation of the amino effect on their photophysical properties in different states, and the utilizations of these compounds in fluorescent sensory and material sciences.

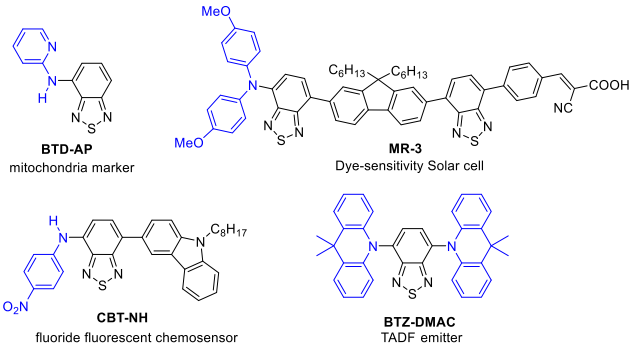

Scheme 1. Representatives of amino substituted BTDs for versatile purposes.

Results and discussion

Synthesis of Am-BTDs (1-7)

Synthetic route to **Am-BTDs** (**1-7**) is shown in Scheme 2. A sequence of Suzuki coupling and Buckwald-Hartwig cross-coupling was applied to prepare **Am-BTDs** (**1-7**). The synthesized compounds could be classified into three categories according to the amino groups, including aliphatic primary amine (**1** and **2**), aromatic primary amine (**3**, **4**, and **5**), and aromatic secondary amine (**6** and **7**). Structures of compounds **1-7** were characterized by ^{1}H NMR, ^{13}C NMR (Figures S1-S14), IR, HRMS, and their single crystal analysis. All compounds are stable to 276 °C according to the thermogravimetric analysis (Figures S15). Decomposition temperatures vary from 276 °C to 355 °C, relying on the amino group (Table 1).

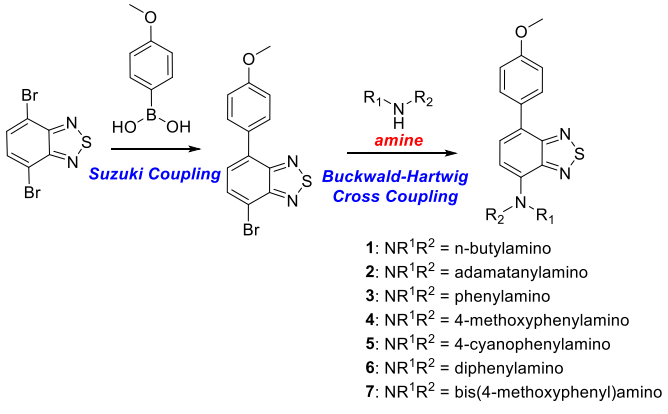

Scheme 2. Synthetic route to compounds **1-7.**

NMR spectra of Am-BTDs (1-7) in $CDCl_3$

The electron donating ability of the various amino groups could be described by the chemical shift of H_a in 2,1,3-benzothiadiazole as illustrated in Figure 1. The chemical shift of H_a in compounds **1-7** is found to be 6.49, 6.87, 7.27, 6.97, 7.55, 7.28, and 6.99, respectively. The smaller the chemical shift is, the greater shielding of this nucleus is. With aliphatic amine substituted, Ha in compounds **1** and **2** are highly shielded in comparison with the ones in aromatic amine substituted compounds **3**-**7**. The best p-π conjugation between lone pair electron of nitrogen and **BTD** core is seen in compound **1**. On the other hand, the chemical shift of H_c could be used to refer to the relative acidity of N-H in compounds **1**-**5**. The larger chemical shift is, the stronger acidity of N-H presents. Thus, compound **5** presents the strongest acidity among these compounds **1**-**5** due to the electron withdrawing nature of the cyano group. Acidities of N-H in compounds **3**-**5** are much stronger than those in compounds **1**-**2** because of the better delocalization of these conjugated bases. Moreover, it is clear that chemical shifts of H_a and H_b in compounds **3** (7.27 and 7.68 ppm) and **6** (7.28 and 7.76 ppm) are almost identical. Similar situation is observed for the pair of compounds **4** and **7**. It indicates that the electronic effect by the replacement of monoarylamino with diarylamino is almost the same no matter how many aryl groups are tethered.

Crystal data of Am-BTDs (1-7)

Fortunately, single crystals of compounds **1-7** were obtained after slow evaporation of their corresponding dilute solutions. Crystallographic data is summarized in Table S1. The selected dihedral angles and bond distances were indicated in Figure 2. In a good accordance with ^{1}H NMR findings, C-N bond length in compounds **1** and **2** is relatively shorter in comparison with those of others. It is found to be 1.366 Å and 1.369 Å for compounds **1** and **2** respectively. This implies that the C-N bond in compounds **1** and **2** has partial double bond character because of the strong electron donating nature of the nitrogen in aliphatic amines. Meanwhile, the conjugation between *para*-methoxyphenyl (**PMP**) and **BTD** is better in compounds **1** and **2** in comparison with those in others, indicated by the dihedral angles between **PMP** and **BTD** as well as the C-C bond lengths between **PMP** and **BTD**. Thus, combining with those findings from ^{1}H NMR, it could be concluded that intramolecular charge transfer (ICT) apparently exist in compounds **1** and **2** no matter whether the state is solution (NMR analysis) or solid (X-ray analysis). However, to the series of compounds **3**, **4**, and **5**, relatively longer C-N bond lengths are observed, especially in the case of compound **5** because of the electron-withdrawing nature of cyano group. Moreover, a more twisted **PMP** is seen in compounds **3**, **4**, and **5** on the basis of the dihedral angles and C-C bond lengths between **PMP** and **BTD**. It implies that the electronic communication between donor and acceptor in these D-A-D molecules (**3**, **4**, and **5**) is weakened which makes these compounds having multipul conformers possible. To the series of compounds **6** and **7**, the three arenes swing around the nitrogen and exist in propeller structure. C-N bond length is determined to be 1.413 Å and 1.410 Å, while the distance between **PMP** and **BTD** is determined to 1.474 Å and 1.477 Å for compounds **6** and **7**, respectively.

View Article Online
DOI: 10.1039/C8TC02416B

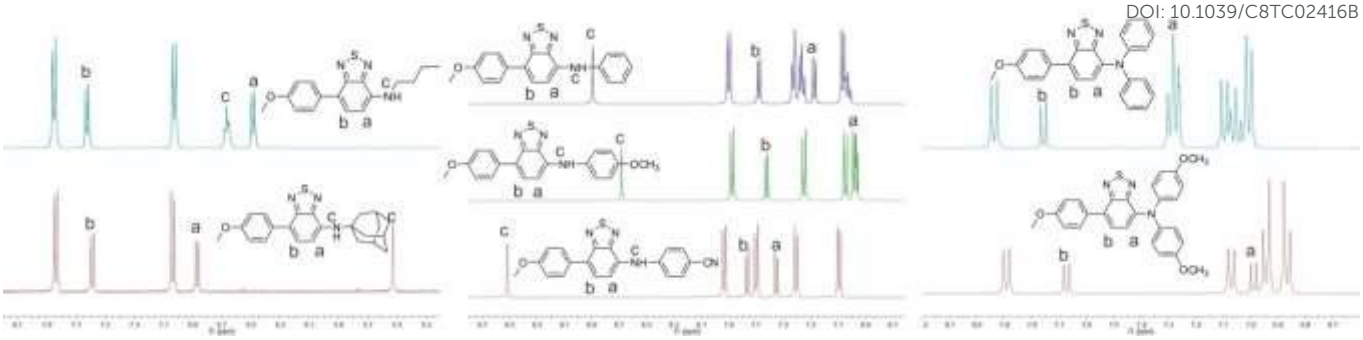

Figure 1. Comparative analysis of ^{1}H NMR spectra of compounds **1-7.**

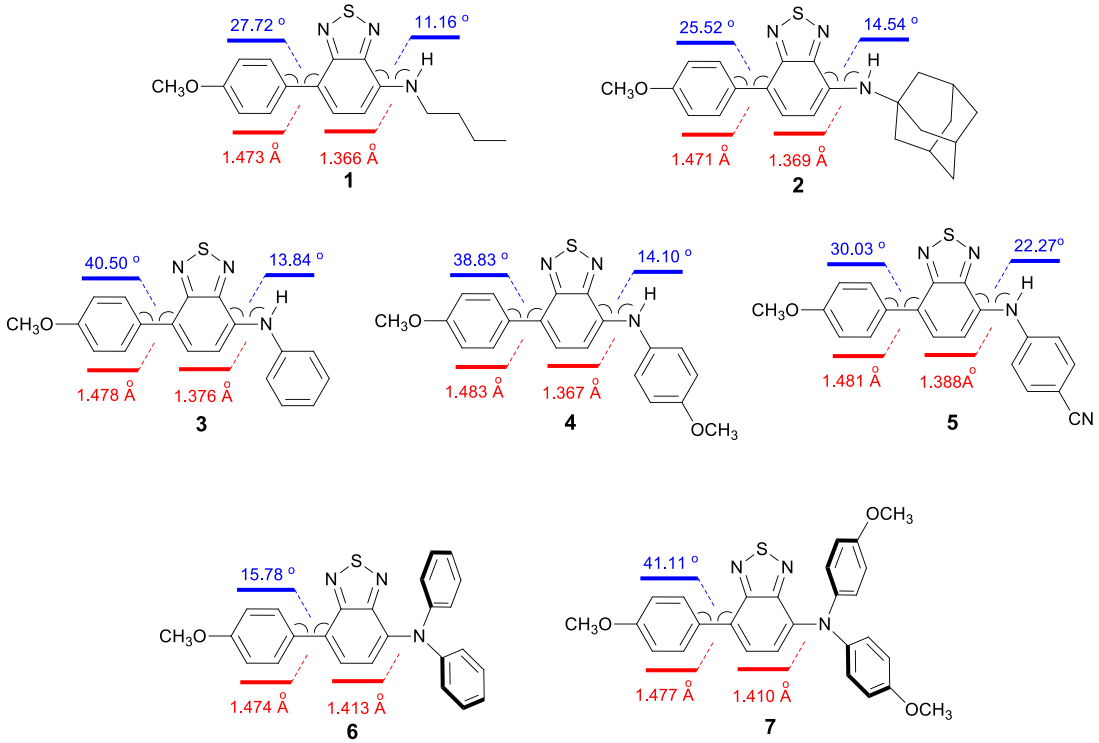

Figure 2. Selected dihedral angles and bond lengths, based on the single crystal analysis.

Absorption of Am-BTDs (1-7) in dilute solutions

At the beginning, we measured the absorption spectra of compounds **1-7** in non-polar toluene solutions in a concentration of 2 x 10^{-5} M (Figure S16, Table 1). With aliphatic amine substituted, compounds **1** and **2** absorb light at 471 nm and 477 nm with molar absorptovities of 6.38 x 10^{3} and 6.43 x 10^{3}, respectively (Figures 3a and S16a). With aniline substituted, compound **3** absorbs light at 475 nm with an increased molar absorptivity of 9.61 x 10^{3}. Addition of methoxy or cyano on the *para*-position of aniline tunes the energy level as we expected. Thus, red-shifted absorption is observed for compound **4**, while blue-shifted absorption is seen for compound **5** (Figure S16b). With one more phenyl or *p*-methoxyphenyl added, the further red-shifted absorption is observed. Thus, compounds **6** and **7** absorb light at 479 nm and 502 nm, respectively (Figure S16c). When the absorption spectra were measured in polar solvent, such as acetonitrile, all compounds presented blue-shifted absorptions with decreased molar absorptivities, respectively (Figure 3b, Figures S16d-f, Table 1).

In compounds **1-7**, **BTD** works as the electron acceptor, while *p*-methoxyphenyl and amino group function as the electron donors. When these D-A-D compounds dissolved in polar solvents, the HOMO/LUMO energy levels in ground states decreased simultaneously because of the solvation. In more polar solvent, the larger transition energy gap is observed because of the more stabilization of the HOMO level.[19]

Emissions of Am-BTDs (1-7) in dilute solutions

Emission spectra of compounds **1-7** in dilute toluene solutions are recorded in a concentration of 2 x 10^{-5} M, excited at the corresponding maximum absorption wavelengths (Table 1). Compound **1** emits light at 595 nm

View Article Online
DOI: 10.1039/C8TC02416B

Table 1. Absorption and emission of **1**-**7** in solutions and in solids.

compound	λ^{max}_{abs} (nm)			λ^{max}_{em} (nm)							Td[e]
	Tol[a] (ε×104)	MeCN[a] (ε×104)	Film	Tol[a,b] (Φ %)	Stokes	MeCN[a,b] (Φ %)	Stokes	Film (Φ %)	Powder[d]	Crystal[d]	
1	471 (0.638)	469 (0.614)	492	595 (2.5)	124	623 (<0.1)	154	575 (10.8)	601	624	276
2	477 (0.643)	473 (0.587)	493	599 (2.6)	122	620 (<0.1)	147	--[c]	614	638	328
3	475 (0.961)	468 (0.904)	488	582 (12.7)	107	611 (1.0)	136	--[c]	579	608	305
4	483 (0.889)	475 (0.865)	501	600 (10.6)	117	625 (<0.1)	150	--[c]	612	637	327
5	461 (1.364)	449 (1.197)	468	569 (30.0)	108	582 (4.2)	133	559 (7.0)	566	578	351
6	479 (0.906)	468 (0.7)	490	575 (61.0)	96	611 (10.8)	143	602 (43.6)	575	591	299
7	502 (0.819)	490 (0.76)	513	630 (4.1)	128	--[c]	-- [c]	-- [c]	622	629	355

[a] measured at 2 x 10^{-5} mol/L, excited at its maximum absorption wavelength, [b] quantum yield was obtained by using integrating sphere, [c] emission is too weak to be detected, [d] excited at its the maximum absorption wavelength in toluene, [e] T_d was determined at 5% weight lose.

with Stokes shift of 124 nm and a quantum yield of 2.5% (Figure 3a). Emission of compound **2** in toluene is almost identical to that of compound **1** (Figure S16a). In these cases, intramolecular charge transfer (ICT) from aliphatic amine to BTD core occurs in excited state and makes the large Stokes shift possible. With aniline substituted, that eventually retards the electron-donating ability of the nitrogen *via* p-π conjugation between the lone pair electrons of nitrogen and benzene, compound **3** emits light at 582 nm with Stokes shift of 107 nm and a quantum yield of 12.7%. With *p*-methoxyphenyl (PMP) substituted, emission of compound **4** is red-shifted with a larger Stokes shift (117 nm) and a lower quantum yield (10.6%) in comparison with those of compound **3**. On the contrary, in case of cyano substituted, compound **5** emits light at 569 nm with a quantum yield of 30% (Figure S16b). Introduction of one more phenyl group, compound **6** emits light at 575 nm with the smallest Stokes shift (96 nm) and the largest quantum yield (61.0%) in this family. It might be ascribed to the propeller shape of triphenylamine (TPA) and thus partially inhibited ICT. Compound **7** emits light at the farthest (630 nm), but with a much lower quantum yield (4.1%) (Figure S16c). In general, the larger Stokes shift is, the lower quantum yield is obtained.[20] Emissions of compounds **1**-**6** in dilute acetonitrile are all red-shifted to those of emissions in toluene (Figure 3b, Figures S16d-f). In the excited state, the polar solvent tends to stabilize the LUMO level and decreases the energy gap. As a result, these compounds present large Stokes shifts in acetonitrile (133 nm ~ 154 nm) but with significantly decreased quantum yields. Some of them present weak luminescence in polar solvent and their emission efficiencies are too weak to be detected, such as compounds **1**, **2**, and **4**. As an extreme example, compound **7** is non-fluorescent in acetonitrile.

Excitation dependant emission (EDE)

Excitation dependant emissions are observed (Figure 3, Figure S17). To compound **1**, two distinguishable emissive peaks are recorded in toluene as well as in acetonitrile as the excitation wavelength changes. In toluene, as the excitation wavelength changes from 380 nm to 440 nm, the emission intensity at shorter wavelength (483 nm) gradually decreases while the emission intensity at longer wavelength (595 nm) increases (Figure 3c). The emissive color change could be seen by naked eye (Figure 3h). It is worthwhile to note that a bright white emission is recorded when this dilute toluene solution is excited at 400 nm. In acetonitrile, these two emissive bands (547 nm and 623 nm) still exist as the excitation wavelength changes from 380 nm to 440 nm (Figure 3d). Similar situation is observed for compound **2** (Figures S17a and S17A). To compound **3**, only one emissive band at lower energy gap (582 nm) is seen in toluene as the excitation wavelength changes from 360 nm to 420 nm. In this case, the emission peak is not shifted, but with a gradually increment of emission intensity (Figure S17b). In acetonitrile, the two emissive bands (545 nm and 611 nm) come back (Figure S17B). This phenomenon is reproducible in case of compound **4** (Figures S17c and S17C). To compound **5**, one emissive peak (569 nm) is recorded with tunable emission intensities as the excitation wavelength changes (Figure S17d). However, a gradually red-shifted emission, accompanied by a decrement of emission intensity, is observed as the excitation wavelength changes from 380 nm to 440 nm (Figure S17D). When compound **6** is examined, only one emissive peak is recorded either in toluene or in acetonitrile (Figures S17e and S17E). Emission spectrum of

View Article Online
DOI: 10.1039/C8TC02416B

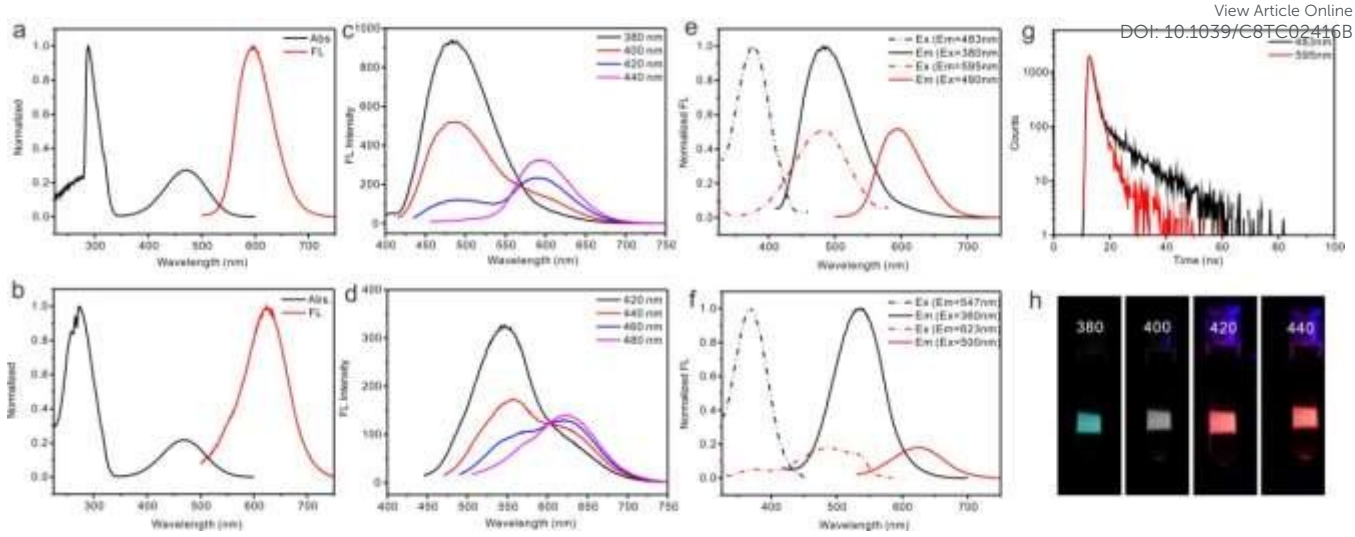

Figure 3. Absorption and emission (excitation at maximum absorption wavelength) of **1** in toluene (a) and in acetonitrile (b); excitation dependent emission of **1** in toluene (c) and in acetonitrile (d); excitation spectra of **1** (monitored at two emissive bands as indicated in parenthesis) in toluene (e) and in acetonitrile(f); fluorescent decay of **1** in toluene with the emission wavelength at 483nm or 595nm; (h) photo of **1** in toluene with different excitation wavelength.

compound **7** in toluene depends upon the excitation wavelength with the appearance of two changeable emissive peaks (Figure S17f). However, emission in acetonitrile is too weak to be detectable. Moreover, emission quantum yields of compounds **1**, **2**, and **7** in dilute toluene solutions are closely related to their excitation wavelengths. For instance, when compound **1** is excited at 380 nm, 400 nm, 420 nm, and 440 nm, emission quantum yield is determined to be 9.0%, 2.5%, 1.2%, and 0.6%, respectively. Similar results are observed for compounds **2** and **7** (Table S2).

These dual emissions are quite unusual and intriguing in comparison with the normally observed two emissions bands from D-A compounds. To a common D-A compound, dual emission bands originate from the locally excited emission (S_1^{LE} emission) and intramolecular charge transfer emission (S_1^{ICT} emission) due to the conformational change in the excited state which should be independent with the excitation wavelength.[21] In order to understand the origin of these dual emissions, we firstly measured the purity of sample in order to avoid the incorrect assessment which may result from the impurity.[22] To all of compounds we investigated, the purity is guaranteed good enough for photophysical study on the basis of HPLC analysis (Figures S18). Secondly, we recorded excitation spectra for each of two emission bands (Figure 3 and Figure S19). To a typical D-A compound, the S_1^{ICT} state could not be directly excited, and it is populated via S_1^{LE} state. Thus, their excitation spectra monitored at two emission bands should be similar and match with its absorption.[23] However, to compound **1**, both excitation spectra show a distinguishable band when monitored either at longer (595 nm) or at shorter wavelength (483 nm) in toluene (Figure 3e). When the excitation spectra are recorded in acetonitrile, two bands are observed in excitation spectrum when monitored at 623 nm, while only one band exists in excitation spectrum when monitored at 547 nm (Figure 3f). Similar situation is recorded for compound **2** (Figures S19a and S19A). In case of compound **5** in acetonitrile, a much broad excitation peak is recorded which is accordance with the excitation-dependent red-shifted emission (Figure S19D and Figure S17D). On the basis of the measurement of the excitation dependent emission and their corresponding excitation spectra, it could be preliminary concluded that the two emissive bands could be respectively excited and the lower energy state is not populated from the higher energy state.

Then we move to the measurement of the lifetimes of these dual emissions (Figure 3g, Figure S20, and Table S2). Figure 3g presents the fluorescence decay traces of compound **1** in toluene recorded in emission at 483 nm and 595 nm, respectively, corresponding to the dual emissions in Figure 3c. Both decay traces are bi-exponential with lifetime components of 1.32 ns (66.32%) and 10.96 ns (33.36%) for emission band at 483 nm, 1.65 ns (90.83%) and 4.85 ns (9.17%) for emission band at 595 nm. To compound **1** in acetonitrile, emission is too weak for the life time measurement. To compound **3** in toluene, one emission band at 582 nm (Figure S17b) fits single exponential with fluorescent lifetime of 4.01 ns. Meanwhile, the two emission bands (Figure S17B) fit bi-exponential function with lifetimes of 1.11 ns (14.81%) and 12.67 ns (85.19%) for emission at 545 nm, 0.94 ns (93.11%) and 5.50 ns (6.89%) for emission at 611 nm, respectively. To compound **5** in toluene, emission at 569 nm fits single exponential with lifetime of 6.84 ns, while two components are recorded for compound 5 in acetonitrile with 2.11 ns (52.98%) and 12.38 ns (47.02%), respectively (Figure S17D). To compound **6**, single emission peak is seen in toluene (575 nm) and in acetonitrile (611 nm) (Figures S17e and S17E). Both of them fit single-exponential function with lifetimes of 15.26 ns and 6.80 ns, respectively. Finally, it could

be concluded that the emission at higher energy gap presents longer lifetime than the emission at lower energy gap.

On the basis of above observations, it is clear that compounds **1**-**7** present excitation dependant emission (EDE) and could be classified into three categories: (a) dual emissions with variable emission intensities (**1-4, 7**), (b) single emission with variable emission intensity (**6**), and (c) gradually red-shifted emission (**5**). These phenomena eventually break the Kasha-Vavilov rule, which states that polyatomic molecules generally luminescence with appreciable yield only from the lowest excited state of a given multiplicity, irrespective of the initial photoexcited state.[23-24] Emission at longer wavelength could be ascribed to $S_1 \rightarrow S_0$ decay as usual D-A molecules present ICT emission, while emission at shorter wavelength could be ascribed to $S_2 \rightarrow S_0$ decay.[25] The variable quantum yield as a function of excitation wavelength further proves the anti-Kasha behavior (Table S2).[26]

To a typical fluorescent molecule, internal conversion (IC) and vibration relaxation (VR) are faster than radiative and other non-radiative decay (Scheme 3). Thus, population in S_1 state occurs which finally results in the emission from S_1 state. In cases of compounds **1** and **2**, dual emissions are seen in both toluene and in acetonitrile because of the strongest electron-donating ability of aliphatic amines which leads to the most charge transfer and the most planarization of molecule among these compounds. As a result, the vibrational relaxation (VR) and the internal conversion (IC) from $S_2 \rightarrow S_1$ are effectively inhibited in these rigid molecules and the emissions from S_2 state come into being. To compounds **3** and **4** in toluene, emissions from S_2 state are effectively inhibited because of the extend conjugation of aryl amine which retards the electron donating ability of nitrogen to **BTD** core. However, in acetonitrile, the intramolecular charge transfer is enhanced *via* the acetonitrile solvation. Thus, emission from S_2 state comes back. To compound **5**, it is actually a D-A-D-A system. Addition of cyano group makes the conformation in excited states more complicated. The resulting multiple conformers bring about red-shifted emissions in acetonitrile as the excitation wavelength changes. In comparison with compound **3**, compound **6** presents single emission in either toluene or acetonitrile because of the propeller structure of triarylamine and the disappearance of the rigid structure. In another word, to these compounds, the appreance of the anti-Kasha emission is depending on the conformation. Rigid conformation tends to present the anti-Kasha emission because of the inhibitted vibrational relaxation (VR) and the internal conversion (IC).

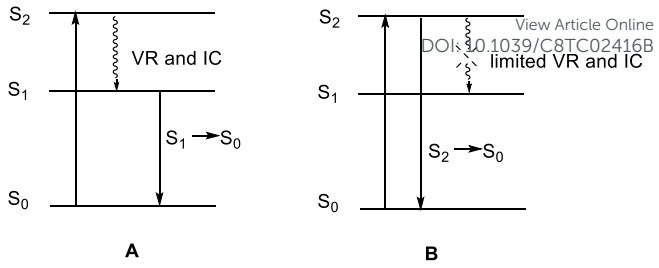

Scheme 3. Illustration of the appearance of emission at larger energy gap.

Emissions of Am-BTDs (1-7) in solids as well as in frozen states

Compounds **1**-**7** are all emissive in powders and in crystals (Table 1, Figure S21).[27] Emissions in crystals are all red-shifted in comparison with the emissions in powders as we can see from the emission spectra (Figure S21) and the photos under UV light (Figure 4). The largest red-shifted emission (29 nm) from powder to crystal is observed for compound **3**.

Emissions of compound **2** are red-shifted in comparison with those of compound **1** in powder and in crystal. It could be explained by the different molecular packing mode in single crystal (Figure 5). To compound **1**, two molecules vertically align in anti-parallel, driven by the π-π stacking (3.390 Å) between two individual **BTD** cores (Figure 5a). Meanwhile,

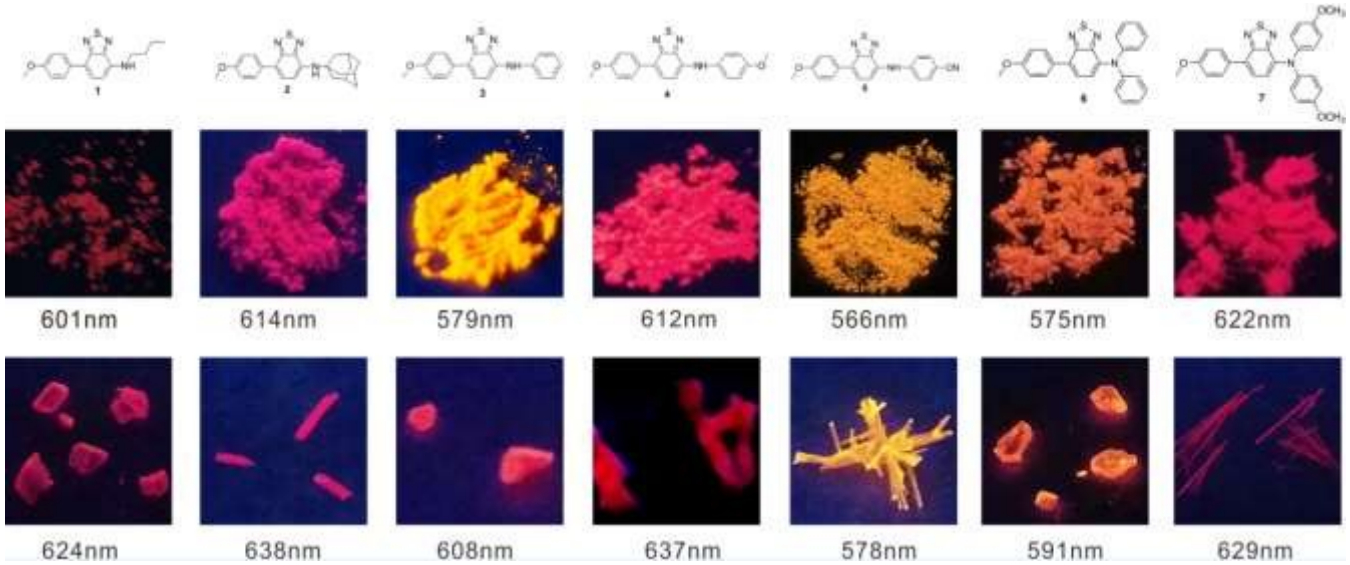

Figure 4. Chemical structures of compounds **1-7** (first row); pristine powders of compounds **1-7** under UV lamp (365 nm) (second row); crystalline states of compounds **1-7** under UV lamp (365 nm) (third row). The numbers indicate their corresponding maximum emission wavelengths.

View Article Online
DOI: 10.1039/C8TC02416B

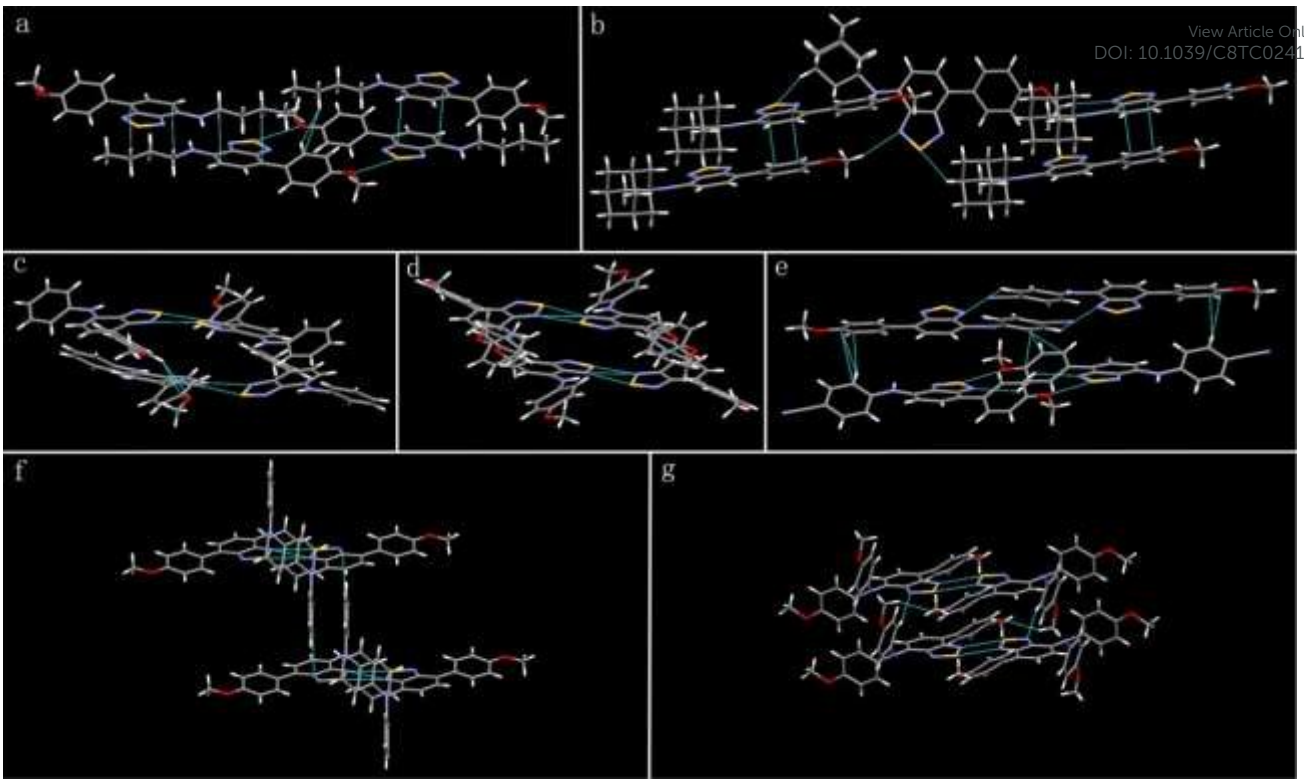

Figure 5. Molecular packing in single crystals of **1** (a), **2** (b), **3** (c), **4** (d), **5** (e), **6** (f), and **7** (g).

two molecules horizontally align in anti-parallel, driven by the short contact between the oxygen of methoxy and the sulfur of BTD (3.125 Å) and multiple C-H…π interactions (2.353 Å, 2.873 Å, 2.832 Å, and 2.886 Å). To compound **2**, because of the ball structure of amantadine, the π-π interaction between the adjacent two **BTD** rings is effectively inhibited, with a parallel but translational alignment of two molecules (Figure 5b). The main intramolecular interaction is the electrostatic force arising from C-H of benzene in **PMP** and π electron circulation of **BTD**. The distance of this CH…π interaction is determined to be 2.960 Å. Other interactions are CH…N interaction (2.654 Å) between methoxy and **BTD**, CH…S interaction (2.931 Å) between amantadine and **BTD**. The parallel alignment of compound **2** induces the red-shifted emission, while the anti-parallel alignment of compound **1** results in the blue-shifted emission.

In the single crystals of compound **3**, **4**, and **5**, multiple conformers are seen. Four conformers exist in the single crystal of compound **3**, while two conformers for **4** and **5**, respectively. The four conformers in compound **3** exist in two layers, each of which possesses an anti-parallel dimer because of the double short-contact between sulfur and nitrogen from the adjacent two **BTD** cores. Further intermolecular CH…O and CH…N interactions integrate these dimers in layer by layer (Figure 5c). The molecular packing mode in compound **4** is similar to what we have seen in compound **3** (Figure 5d). However, in the case of compound **5**, the double short-contact between sulfur and nitrogen is absent because of the insertion of the cyano group (Figure 5e). Crystal densities of compounds **3**, **4**, and **5** are determined to be 1.387, 1.416, and 1.435 g cm^{-3}, respectively (Table S1). It implies that compound **3** is of the largest tendency to change the emissive color in solid states among these compounds by applying external stimuli.[28] Molecular packing mode is essentially the same in single crystals of compound **6** (Figure 5f) and compound **7** (Figure 5g). The double short-contact between sulfur and nitrogen from the two adjacent **BTD** cores results in a dimer with anti-parallel alignment and further assembles to contruct a layer-by-layer structure through CH…π interaction in compound **6** and CH...N interaction in compound **7**.

Films are formed by spinning the dilute chlorobenzene solution of compounds **1**-**7** on quartz plates and then being vaporized under atmosphere. Absorptions of compounds **1**-**7** in films are all red-shifted about 20 nm to those absorptions in dilute acetonitrile solutions with larger full widths at half maximum intensity (FWHMs) (Table 1, Figure S22). Three films, prepared from **1**, **5**, and **6**, are fluorescent while others are not. These three films emit light at 575 nm, 559 nm, and 602 nm with quantum yields of 10.8%, 7.0%, and 43.6%, respectively. By doping these compounds in PMMA (9 x 10^{-5} mol **1**-**7** / 1 g PMMA), the films, doped with compounds **5** and **6**, are fluorescent and emit light at 563 nm and 571 nm, respectively. Others are non-fluorescent (Figure S23).

As the excitation wavelength changes from 360 nm to 420nm, all powders (**1**-**7**) show a single emission (Figures S24). This is a good indicative of the expression of anti-Kasha's emission in the solution. In the condensed phase, the energy released from VR and IC processes could be relieved as heat through intermolecular interactions which directly results in the

View Article Online
DOI: 10.1039/C8TC02416B

depopulation of S_2 states.[23] In another word, only one emission band ($S_1 \rightarrow S_0$) could be seen in the condensed phase. Similar situation is observed for their emissions in frozen state. By freezing the dilute toluene solutions of compounds **1-7** in liquid nitrogen, only one emission band ($S_1 \rightarrow S_0$) is observed and the intensity changes as the excitation wavelength changes (Figure S25).

Application as gaseous ammonia sensor

Absorption and emission spectra of compounds **1**-**6** rely on the environmental acidity (Figure S26). When the absorption spectra of these compounds are recorded in acetonitrile in the presence of 0.1 M HCl, blue-shifted absorption is observed for compounds **1** and **2**. As we can see from the photo (Figure 6a, inset photo), the yellow color fades in the presence of HCl. Nevertheless, the emission turns on. Bright yellow emission is seen when HCl is added to the acetonitrile solution of compound **2**. The quantum yield is determined to be 22.2% for **2** in acidic acetonitrile. The distinguishable emission color change of compound **2** could be used to reversibly probe gaseous hydrogen chloride and gaseous ammonia (Figure S27).[29] Dipping the fluorescent silica plate (Silica GF254) into dilute dichloromethane solution of compound **2** and evaporating the solvent, a pristine plate with the doping of compound **2** is prepared. The pristine plate is blue under UV light. Putting the pristine plate on the top of the bottle of the concentrated HCl and saturating with HCl vapor for 180 seconds, the plate becomes yellow under UV light. The color could be turned back to blue after the plate is re-saturated with ammonia vapor for 30 seconds. As a practical usage, the powder of compound **2** could be directly used to detect ammonia and hydrogen chloride vapor in a reusable way (Figures 6b and 6c). The color of the powder changes between yellow and red under UV light when the powder is alternatively exposure to hydrogen chloride and ammonia vapor for 180 seconds and 30 seconds, respectively.

Application as fluoride anion sensor

These compounds are versatile. Compound **5** might be developed as a potential fluoride fluorescent chemosensor due to the enhanced acidity of the NH group affected by the electron withdrawing cyano group which is absent in other compounds (Figure 7). Absorption spectrum changes as

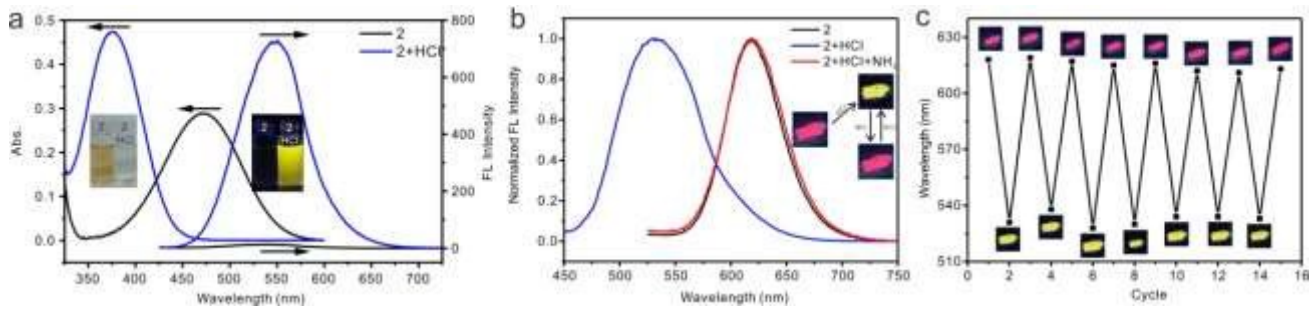

Figure 6. (a) Acidity effect on absorption and emission of **2** in MeCN. Inset: photo before and after adding acid under day light and UV light (365nm); (b) Emission of powder **2**, exposed to HCl and NH_3 vapor; (c) Reversible color change of powder **2** under alternative exposure to HCl and NH_3 vapor for 180 and 30 s, respectively (ex 365nm).

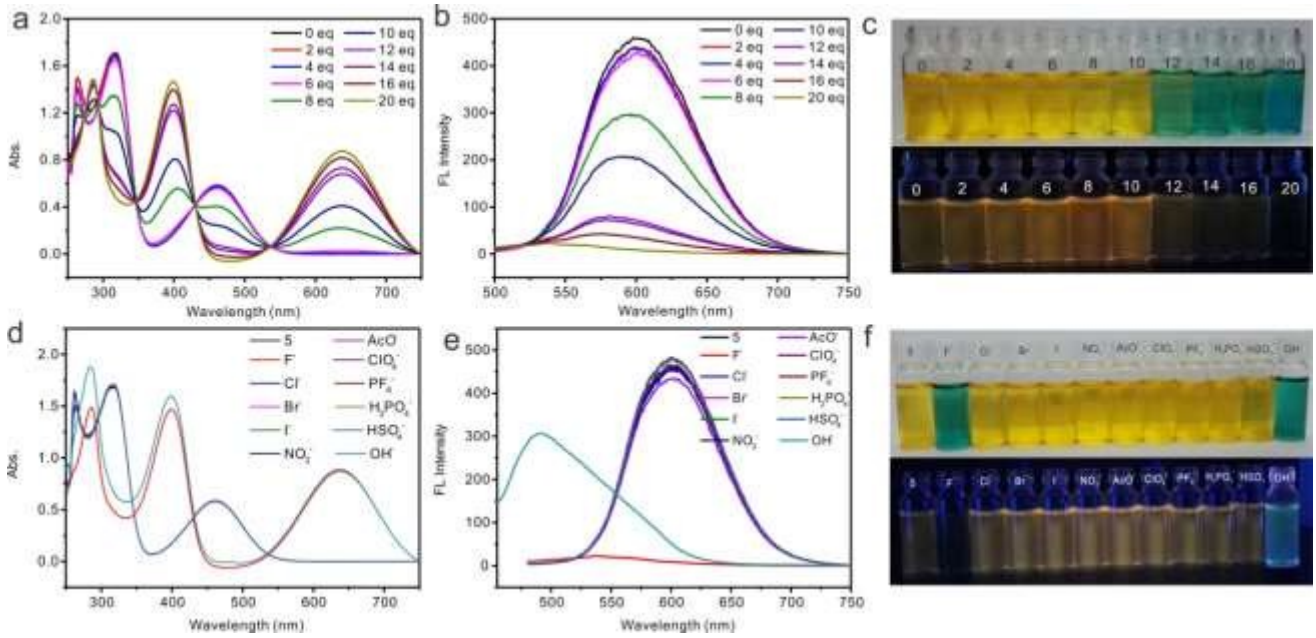

Figure 7. Absorption (a), emission (b), and photo (c) of **5** (c = 5 x 10^{-5} M, DMSO) in the presence of varied amounts of TBAF; Absorption (d), emission (e), and photo (f) of **5** (5 x 10^{-5} M, DMSO) in the presence of 20 equivalents of various tetrabutylammonium salts in DMSO.

tetrabutylammonium fluoride gradually approaches to 20 equivalents to compound **5** (Figure 7a). Three isobestic points appear in absorption spectra with values of 347, 430, and 536nm, respectively. Solution color stays yellow as the fluoride anion reaches to 10 equivalents. A dramatic change is observed when the fluoride anion reaches to 12 equivalents. The color changes to green and keeps the same beyond this point (Figure 7c). Meanwhile, a turn-off emission is observed as fluoride anion adds to the dilute solution of compound **5**. When the fluoride anion reaches 10 equivalents, the emission intensity decreases to half of its initial. As the amount of fluoride anion further increases, the emission intensity decreases and finally turns off at 20 equivalents (Figure 7b).

Subsequently, we tested the anion selectivity. Thus, various anions are respectively added to the dilute solution of compound **5**. Absorption spectra keep unchanged when Cl^-, Br^-, I^-, NO_3^-, AcO^-, ClO_4^-, PF_6^-, $H_2PO_4^-$, HSO_4^- are respectively tested except the hydroxide anion (Figures 7d and 7f). As the gradual addition of the hydroxide anion, the absorption spectrum alters and the alternation is almost identical to the addition of fluoride anion (Figure 7d). Fortunately, the discrimination between fluoride and hydroxide anions could be realized by the measurement of their emission spectra (Figures 7e and 7f). Addition of hydroxide leads to a blue-shifted emission, while addition of fluoride turns emission off.

Electrochemical studies of Am-BTDs (1-7)

Oxidation and reduction potentials obtaining from cyclic voltammetry are applied to estimate the frontier orbital levels and the results are summarized in Figure S29 and Table S4. The energy gaps between HOMO and LUMO obtaining from electrochemical study are in good accordance with the energy gaps resulting from UV measurements except for the cases of compound **1** and **4**. Meanwhile, the results obtaining from the theoretical calculation (Figure S28,S30) are in good accordance with those from UV measurements in tendency, but with much higher absolute values.

Electroluminescence of compound 6

To further extend the utility of these compounds, an organic light emitting diode with a structure of ITO / PEDOT:PSS (40 nm) / compound **6** (65 nm) / TBPI (40 nm) / LiF (1.5 nm) / Al (50 nm) is fabricated. The device emits light at 625 nm (CIE: 0.63, 0.37) with HWHM of 107 nm at voltage of 7 V and exhibits a turn-on voltage of 3.0 V at a brightness of 1 cd m^{-2}, external quantum efficiency (EQE) of 0.91 %, luminous efficiency of 1.06 cd A^{-1} and power efficiency of 0.81 lm W^{-1} (Figure 8).

Conclusions

In conclusion, by directly covalent bonding amino group to **BTD** core, we have developed a series of **Am-BTDs** with interesting and applicable fluorescent properties. Anti-Kasha's emission is observed for some **Am-BTDs** in solutions which could be ascribed to the strong electronic

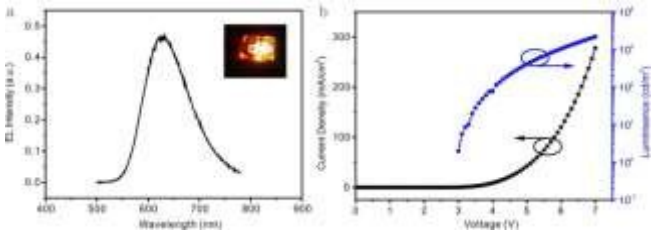

Figure 8. (a) EL spectra of **6**-based device operating at voltage of 7V. Inset: Image of device; (b) Current density-Luminance–Voltage (L–J–V) characteristics.

communication between nitrogen and **BTD** core. The stronger the electronic communication is, the more expression of anti-Kasha's emission. Applying this abnormal property, a white solution emission is approached. Moreover, some **Am-BTDs** could be developed as fluorescent pH sensors for detecting environmental acidity, not only for probing the solution acidity but also for probing the gaseous ammonia. It is also noteworthy that compound **5** could be developed as a fluorescent fluoride sensor. The discrimination between fluoride and hydroxide could be easily achieved by the fluorescent detection. Finally, **Am-BTDs** are not only emissive in solutions but also emissive in solids. Emissive color in solid is tunable and varies from yellow to red depending on the different amino groups as well as the different states. In film state, a maximum quantum yield of 43.6% is approached which opens a window for them to become the promising emitting materials in OLEDs. Although the OLED result is not good enough at this stage, the facile preparation, the tunable color, the abnormal anti-Kasha's emission and the thermal stability of these new compounds are valuable and worthwhile to note in the future.

Conflicts of interest

The authors declare no conflict of interest.

Acknowledgements

The authors thank Prof. Yizheng Jin for providing the convenience in the fabrication of OLED device and thank the national natural science foundation of China (21472173).

Notes and references

1 C. D. Müller, A. Falcou, N. Reckefuss, M. Rojahn, V. Wiederhirn, P. Rudati, H. Frohne, O. Nuyken, H. Becker, K. Meerholz, *Nature*, 2003, **421**, 829.

2 (a) H. N. Tsao, D. M. Cho, I. Park, M. R. Hansen, A. Mavrinskiy, D. Y. Yoon, R. Graf, W. Pisula, H. W. Spiess, K. Müllen, *J. Am. Chem. Soc*., 2011, **133**, 2605; (b) M. Zhang, H. N. Tsao, W. Pisula, C. Yang, A. K. Mishra, K. Müllen, *J. Am. Chem. Soc.*, 2007, **129**, 3472; (c) B. P. Sonar, S. P.

Singh, Y. Li, M. S. Soh, A. Dodabalapur, *Adv. Mater.*, 2010, **22**, 5409.
3 (a) Y. Li, *Acc. Chem. Res.*, 2012, **45**, 723; (b) J. Du, M. C. Biewer, M. C. Stefan, *J. Mater. Chem. A*, 2016, **4**, 15771; (c) Q. Liu, H. Zhan, C.-L. Ho, F.-R. Dai, Y. Fu, Z. Xie, L. Wang, J.-H. Li, F.Yan, S.-P. Huang, W.-Y. Wong, *Chem. Asian J.*, 2013, **8**, 1892.
4 W. Duan, J. Huang, J. A. Kowalski, I. A. Shkrob, M. Vijayakumar, E. Walter, B. Pan, Z. Yang, J. D. Milshtein, B. Li, C. Liao, Z. Zhang, W. Wang, J. Liu, J. S. Moore, F. R. Brushett, L. Zhang, X. Wei, *ACS Energy Lett.*, 2017, **2**, 1156.
5 J. Chen, C.-L. Dong, D. Zhao, Y.-C. Huang, X. Wang, L. Samad, L. Dang, M. Shearer, S. Shen, L. Guo, *Adv. Mater.*, 2017, DOI: 10.1002/adma.201606198.
6 (a) B. A. D. Neto, P. H. P. R. Carvalho, J. R. Correa, *Acc. Chem. Res.*, 2015, **48**, 1560; (b) P. H. P. R. Carvalho, J. R. Correa, B. C. Guido, C. C. Gatto, H. C. B. D. Oliveira, T. A. Soares, B. A. D. Neto, *Chem. Eur. J.*, 2014, **20**, 15360.
7 J. Wu, G. Lai, Z. Li, Y. Lu, T. Leng, Y. Shen, C. Wang, *Dyes and Pigments*, 2016, **124**, 268.
8 Q. Ye, S. Chen, D. Zhu, X. Lu, Q. Lu, *J. Mater. Chem. B*, 2015, **3**, 3091.
9 D. Raychev, O. Guskova, *Phys.Chem.Chem.Phys.*, 2017, **19**, 8330.
10 (a) J. T. Bloking, X. Han, A. T. Higgs, J. P. Kastrop, L. Pandey, J. E. Norton, C. Risko, C. E. Chen, J.-L. Brédas, M. D. McGehee, A. Sellinger, *Chem. Mater.*, 2011, **23**, 5484; (b) H.-I. Lu, C.-W. Lu, Y.-C. Lee, H.-W. Lin, L.-Y. Lin, F. Lin, J.-H. Chang, C.-I. Wu, K.-T. Wong, *Chem. Mater.*, 2014, **26**, 4361.
11 (a) S. Chen, N. Chen, Y. L. Yan, T. Liu, Y. Yu, Y. Li, H. Liu, Y. S. Zhao, Y. Li, *Chem. Commun.,* 2012, **48**, 9011; (b) A. A. Vieira, R. Cristiano, A. J. Bortoluzzi, H. Gallardo, *J. Mol. Struct.*, 2008, **875**, 364.
12 (a) J. Zhang, W. Chen, A. J. Rojas, E. V. Jucov, T. V. Timofeeva, T. C. Parker, S. Barlow, Seth R. Marder, *J. Am. Chem. Soc.*, 2013, **135**, 16376; (b) J. Liu, L. Bu, J. Dong, Q. Zhou, Y. Geng, D. Ma, L. Wang, X. Jing, F. Wang, *J. Mater. Chem.*, 2007, **17**, 2832; (c) M. Kimura, M. Karasawa, N. Sasagawa, K. Takemoto, R. Goto, S. Mori, *Chem. Lett.*, 2012, **41**, 1613.
13 (a) J. W. Jung , F. Liu , T. P. Russell, W. H. Jo, *Adv. Mater.*, 2015, **27**, 7462; (b) M. Wang, D. Cai, Z. Yin, S.-C. Chen, C.-F. Du, Q. Zheng, *Adv. Mater.*, 2016, **28**, 3359; (c) J.-L. Wang , F. Xiao, J. Yan, Z. Wu, K.-K. Liu, Z.-F. Chang, R.-B. Zhang, H. Chen, H.-B. Wu, Y. Cao, *Adv. Funct. Mater.*, 2016, **26**, 1803; (d) Z. Li, J. Lu, S.-C. Tse, J. Zhou, X. Du, Y. Tao, J. Ding, *J. Mater. Chem.*, 2011, **21**, 3226; (e) Y. Liu, W. Zhao, Y. Wu, J. Zhang, G. Li, W. Li, W. Ma, J. Hou, Z. Bo, *J. Mater. Chem. A*, 2016, **4**, 8097; (f) L. Cartwright, A. Iraqi, Y. Zhang, T. Wang, D. G. Lidzey, *RSC Adv.*, 2015, **5**, 46386.
14 A. Casey, S. D. Dimitrov, P. Shakya-Tuladhar, Z. Fei, M. Nguyen, Y. Han, T. D. Anthopoulos, J. R. Durrant, M. Heeney, *Chem. Mater.*, 2016, **28**, 5110.
15 (a) D. L. Crossley, I. A. Cade, E. R. Clark, A. Escande, M. J. Humphries, S. M. King, I. Vitorica-Yrezabal, M. J. Ingleson, M. L. Turner, *Chem. Sci.*, 2015, **6**, 5144; (b) D. L. Crossley, R. Goh, J. Cid, I. Vitorica-Yrezabal, M. L. Turner, M. J. Ingleson, *Organometallics*, 2017, **36**, 2597.
16 (a) S. Zeng, L. Yin, C. Ji, X. Jiang, K. Li, Y. Li, Y. Wang , *Chem. Commun.*, 2012, **48**, 10627; (b) H.-H. Chou, Y.-C. Chen, H.-J. Huang, T.-H. Lee, J. T. Lin, C. Tsai, K. Chen, *J. Mater. Chem.*, 2012, **22**, 10929.
17 B. A. D. Neto, P. H. P. R. Carvalho, D. C. B. D. Santos, C. C. Gatto, L. M. Ramos, N. M. de Vasconcelos, J. R. Corrêa, M. B. Costa, H. C. B. de Oliveira, R. G. Silva, *RSC Adv*, 2012, **2**, 1524.
18 F. Ni, Z. Wu, Z. Zhu, T. Chen, K. Wu, C. Zhong, K. An, D. Wei, D. Ma, C. Yang, *J. Mater. Chem. C*, 2017, **5**, 1363.
19 N. S. Bayliss, E. G. McRae, *J. Phys. Chem.*, 1954, **58**, 1002.
20 M. K. Singhi, H. Pal, A. C. Bhasikutta, A. V. Sapre, *Photochem Photobiol*, 1998, **68**, 32.
21 (a) J. Catalán, *Phys. Chem. Chem. Phys.*, 2013, **15**, 8811; (b) K. Santhosh and A. Samanta, *ChemPhysChem*, 2012, **13**, 1956.
22 P. Suppan, S. Huber, E. Haselbach, *Helv. Chim. Acta.*, 1983, **66**, 2597.
23 A. P. Demchenko, V. I. Tomin, P.-T. Chou, *Chem Rev*, 2017, **117**, 13353.
24 P. Klán, J. Wirz, *Photochemistry of Organic Compounds: From Concepts to Practice*, Wiley, Chichester, West Sussex, United Kingdom 2009.
25 S. D. Choudhury, S. Muralidharan, H. Pal, *Phys. Chem. Chem. Phys.*, 2014, **16**, 11509.
26 H.-W. Tseng, J.-Y. Shen, T.-Y. Kuo, T.-S. Tu, Y.-A. Chen, A. P. Demchenko, P.-T. Chou, *Chem. Sci.*, 2016, **7**, 655.
27 Q. Li, Z. Li, *Adv. Sci.*, 2017, 4, 1600484.
28 Z. Peng, K. Huang, Y. Tao, X. Li, L. Zhang, P. Lu, Y.Wang, *Mater. Chem. Front.*, 2017, **1**, 1858.
29 Z. Cheng, H. Shi, H. Ma, Li. Bian, Q. Wu, L. Gu, S. Cai, X. Wang, W. Xiong, Z. An, W. Huang, *Angew. Chem., Int. Ed.*, 2018, **57**, 678.

View Article Online
DOI: 10.1039/C8TC02416B

Graphic abstract